
EXPERIMENTAL AND NUMERICAL STUDIES OF OPPOSED JET OXYGEN-ENHANCED METHANE DIFFUSION FLAMES

ZHONGXIAN CHENG
JOSEPH A. WEHRMEYER
ROBERT W. PITZ*

Mechanical Engineering Department, Vanderbilt
University, Nashville, Tennessee, USA

Planar oxygen-enhanced methane counterflow flames are investigated by optical diagnostics and numerical simulation. The major species concentrations and temperature measured from Raman scattering are compared to the detailed simulations of the flame formed between two opposed jets. The effect of stretch and the influence of oxygen concentration in the oxidizer on the flame structure are studied for nitrogen-diluted methane fuel (20% CH₄ in N₂). The oxygen concentration of reactants changes the flame temperature dramatically. Simulations with the GRI-3.0 and the San Diego chemical kinetic mechanisms show that model-data comparisons for reactants, products such as H₂O, and temperature agree very well. The measured CO₂ is in agreement at lower oxygen enrichment ($\leq 40\%$ O₂) but deviates from prediction at high oxygen enrichment (60%, 100% O₂). The effect of the fuel concentration in the nitrogen-diluted fuel is also studied for pure oxygen flames. When

Received 28 June 2005; accepted 30 January 2006.

This research work was partially supported by Gas Research Institute. Air Products and Chemical, Inc provided most of the gases used in this research. The authors give special thanks for this support.

Zhongxian Cheng is presently at: Institute for Combustion Science and Environmental Technology, Western Kentucky University, Bowling Green, KY 42101, USA.

Joseph A. Wehrmeyer is presently at: Aerospace Testing Alliance, Building 1099, Avenue C, Arnold Air Force Base, TN 37389, USA.

*Address correspondence to robert.w.pitz@vanderbilt.edu

pure oxygen is the oxidizer, the measured extinction limit for the minimum amount of fuel in the diluted fuel mixture is very close to the calculated result when using either the GRI-3.0 or the San Diego chemical kinetic mechanisms. At low-level enrichment (i.e., 30% O₂) and high-level enrichment (100% O₂), the GRI-3.0 and the San Diego mechanisms give almost identical predicted results.

Keywords: counterflow, opposed jet, oxygen-enhanced, planar, stretch

INTRODUCTION

Oxygen-enhanced combustion had been used increasingly in industry over the last two decades to improve productivity and reduce emissions (Baukal, 1998; Pourkashanian et al., 1989). Unlike traditional combustion that uses air (21% O₂ by volume) as an oxidizer, oxygen-enhanced combustion has oxygen concentration varying from 21% to 100%. When 100% O₂ is used as the oxidizer, it is termed an oxy/fuel flame. The fundamental effects of oxygen-enrichment on flame characteristics are high flame temperature, high flame speed, reduced flame length and increased flammability range (Baukal, 1998; Pourkashanian et al., 1989). Burning fuel with pure O₂ instead of air can increase CO₂ concentration in the exhaust gas making CO₂ capture and sequestration more feasible. Theoretically NO_x can be completely eliminated by oxy/fuel combustion. Unfortunately in practical systems, a small percentage of N₂ always exists in the fuel or oxidizer and NO_x emissions can be worse because of thermal NO_x formation at high temperature in the oxygen-enhanced flames (Sung and Law, 1998). The effect of oxygen-enhancement on NO_x and soot formation has been investigated in counterflow flame studies (Leung et al., 1991; Naik and Laurendeau, 2002a, 2002b). In industry, strategies are being proposed to reduce NO_x using oxy/fuel flames (Charon et al., 1993). Recently Qin and co-workers (2000) have studied the effect of O₂ composition modulation on the dynamics and structure of lean CH₄/air premixed flames. They found that the addition of extra O₂ in the oxidizer noticeably extends the lean flammability limit and thus stable combustion can be achieved at leaner conditions, which are also characterized by reduced fuel consumption, lower flame temperatures and reduced NO_x emissions. Nitric oxide formation during oxy/fuel combustion was studied with a counterflow burner by Sung and Law (1998), where pathway and sensitivity analysis were used to identify

key reactions contributing to the production of NO in oxy/fuel combustion and thermal NO was found to dominate.

In oxygen-enriched flames, high flame temperature, strong flame emissions and laser-induced fluorescence (LIF) interference have led to experimental difficulties in determining the flame structure. Except for the optical measurement of NO (Naik and Laurendeau, 2002a, 2002b; Naik et al., 2003) and soot (Beltrame et al., 2001; Vandsburger et al., 1984), few nonintrusive optical experimental data are available for this kind of adverse flame environment. In this work, we use Raman scattering measurement of temperature and major species concentrations to study the various opposed jet oxygen-enhanced flame structures. The oxygen concentration ranges from 21% to 100% and all the flames are non-sooting. Planar opposed jet oxygen-enhanced methane flames are relatively thin and can be simplified into a two-point boundary value problem. The simulation of this kind of flame structure with complete chemical mechanisms can be used to validate the chemical kinetics.

EXPERIMENTAL SYSTEM AND FLAMES EXAMINED

Measurements of major species concentration are made along the centerline of an opposed jet burner using the nonintrusive Raman diagnostic system. The local flame temperature is determined from the major species concentrations using the ideal gas law and the known pressure (1 atm). The laser diagnostic system is similar to that described by Cheng et al. (2002, 2005). A schematic of the visible Raman system is shown in Figure 1. A 532 nm Nd:YAG laser beam is stretched in time from 7 ns to 35 ns with a beam splitter-mirror system and focused by a 0.3 m lens. A Stanford Research Systems DG535 pulse generator synchronizes the trigger signals in the system. The Raman light collecting system described in the previous work (Cheng et al., 2002) is modified by replacing the F/1.5 Cassegrain mirror with a 75 mm diameter F/2 lens. The collimated light from this F/2 lens is focused by a 75 mm diameter F/7.5 lens, passed through a ferroelectric shutter, a mechanical shutter, and an entrance slit to the 0.65 meter focal length spectrometer. A mechanical shutter is used as an external shutter for the liquid nitrogen cooled CCD camera but the shutter has a relatively long exposure time (6 ms). A ferroelectric liquid crystal shutter is placed in front of the mechanical shutter to cut off flame luminosity into the spectrometer by its short exposure time (30 μ s). A Schott orange glass filter is placed in front of

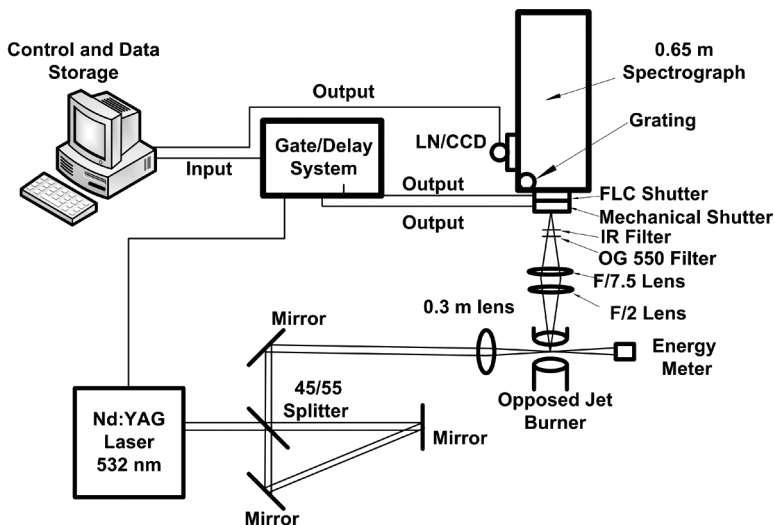


Figure 1. Visible Raman system schematic.

the entrance slit to block any stray 532 nm light. A separate IR filter (750 nm cutoff) is mounted at the entrance slit to eliminate the infrared radiation from the flame. A liquid-nitrogen-cooled, charge-coupled-device (LN/CCD) is used to obtain the Raman spectra.

The LN/CCD camera has a 1024*1024 pixel chip mounted to the back plane of the spectrometer. The chip is back-illuminated to give high quantum efficiency in the visible ($\sim 70\%$). The measuring sample volume is a cylinder (length is 4.7 mm and diameter is 0.2 mm). For the planar flame measurement, the 0.2 mm dimension is transverse to the concentration and temperature gradients. Thus, the 0.2 mm dimension is the spatial resolution of the system. Typical Raman spectra taken in an oxy/fuel flame are shown in Figure 2. This is a pure oxygen flame that has significant interference, particularly on the fuel side of the maximum temperature (Figure 2c, $x = 7.3$ mm).

For the oxygen-enriched flame experiment, a safety system is designed that consists of a control system, solenoid valves, check valves, and a high-pressure purge nitrogen line. If the flame goes out, a solenoid valve automatically cuts off the fuel to ensure no flash-back. The gas lines are cleaned for oxygen service. The opposed jet burner has been modified from the design of Seshadri et al. (1985) and has been used extensively for hydrogen- and hydrocarbon-fueled diffusion flames and for hydrocarbon-fueled

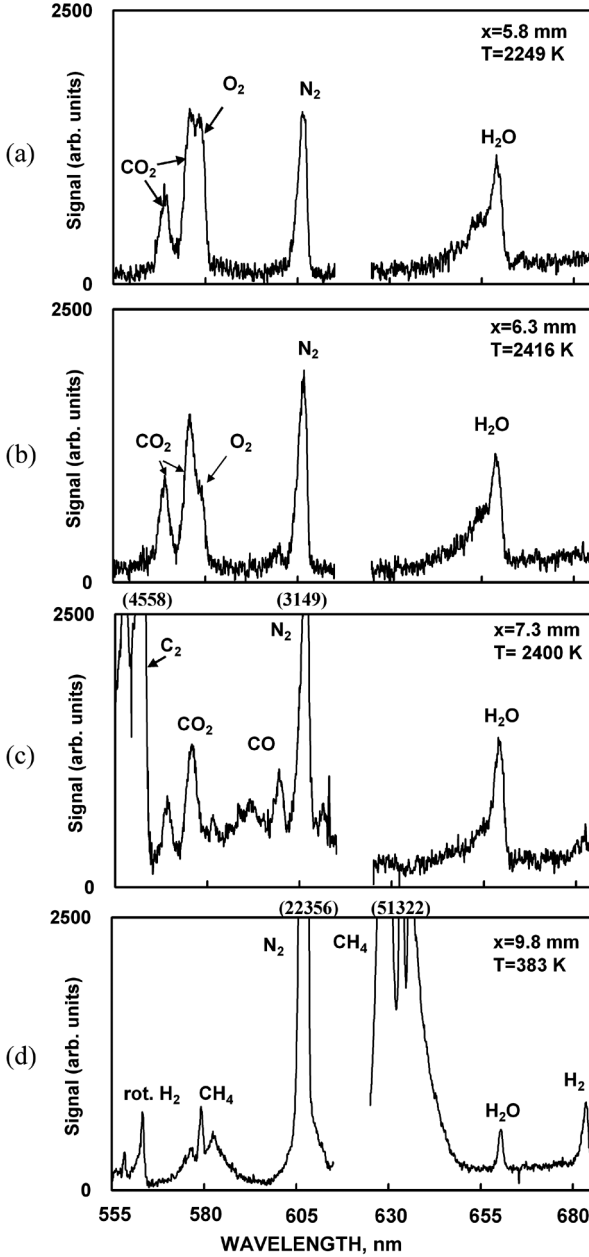


Figure 2. Representative Raman spectra obtained from the flame (100% O₂ vs. 20% CH₄-80% N₂, $\kappa = 60 \text{ s}^{-1}$) shown in Figure 9. Spectra correspond to four axial positions along the centerline of the opposed jet burner where “x” is the distance from the top jet. Some Raman peaks are cut off and their peak values are given in parenthesis.

Table 1. Flame parameters

Group	CH ₄ (Vol., %)	O ₂ (Vol., %)	Stretch rate, κ (s ⁻¹)
A	20	30	60
		31	130
		31	168
B	20	23	60
		40	
		60	
		80	
		100	
C	15	100	60
	10		
	8		

premixed flames. Also the opposed jet burner has been modified by inserting honeycomb metal “flow straighteners” into both 25 mm diameter nozzles. These inserts have 0.8 mm honeycomb cells that are 19 mm in length. The inserts provide a very uniform exit velocity profile for both nozzles, as verified by hot wire anemometry traverses in the nonreacting flow.

Table 1 gives the flame parameters studied in this work. Eleven flames are grouped into three groups by oxygen concentration in the oxidizer jet, methane concentration in the fuel jet or stretch rate. Group A includes three flames that have different stretch rates (60, 130, and 168 s⁻¹) but the same nominal CH₄ and O₂ concentrations. Group B includes five flames that have different oxygen concentrations in the oxidizer (23% to 100%) but have the same stretch rate. Group C includes three pure oxygen flames that have different fuel concentrations in the fuel stream while keeping O₂ concentration and stretch rate constant. The stretch rate is calculated according to: $k = 2V_O/L (1 + V_F\sqrt{\rho_F}/V_O\sqrt{\rho_O})$ (Kim et al., 1992). Here L is the separation distance between the two jets ($L = 12.6$ mm for the current study) and V , ρ are velocity and density of inlet gas streams, respectively. The subscript O indicates the oxidizer stream, and subscript F indicates the fuel stream. The typical boundary conditions for velocity at $\kappa = 60$ s⁻¹ are $V_F = V_O = 19$ cm/s.

NUMERICAL SIMULATIONS AND CHEMICAL MECHANISMS

The diffusion flame formed by two axisymmetric opposed jets can be modeled by the OPPDIF (Kee et al., 2002) application software, which

is part of CHEMKIN package. The numerical simulations employ detailed transport (mixture-averaged formulation) and complex chemistry: GRI-3.0 (Smith et al., 1999) and San Diego (Williams, 2003) chemical kinetic mechanisms. Radiation effects are not included in the model.

RESULTS AND DISCUSSION

Stretch Rate Effect on the Structure of Oxygen-Enhanced Flame

Stretch can affect the diffusion flame structure significantly. The flame thickness, δ , is decreased as the stretch rate, κ , is increased by $\delta \sim (D/\kappa)^{1/2}$ due to the finite diffusion rate, D (Sung et al., 1995). With increasing stretch rate, the reactant residence time is shorter than the chemical reaction time and incomplete reaction will cause the flame to extinguish. In order to see how stretch rate affects the flame structure, oxygen-enhanced flame structures at three stretch rates ($\kappa = 60, 130$ and 168 s^{-1}) are shown in Figures 3–5.

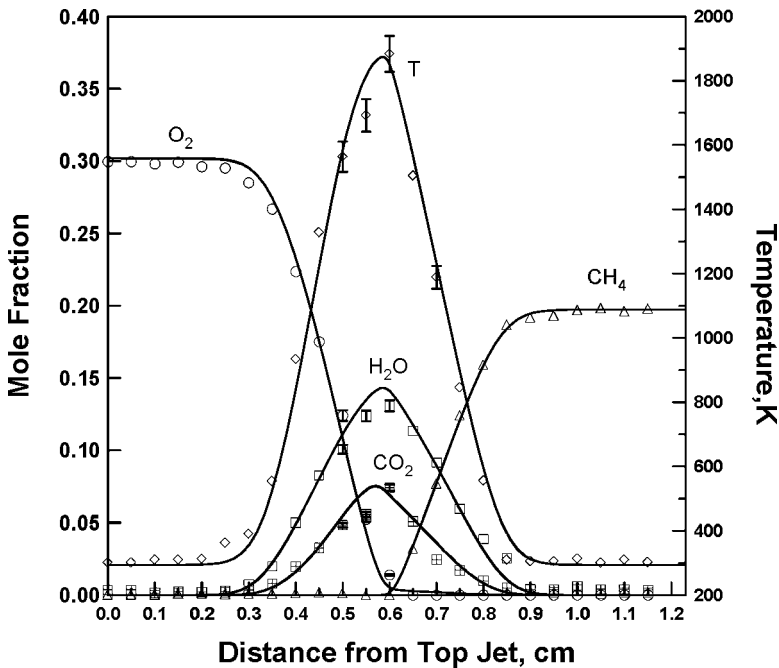


Figure 3. Experimental and numerically-predicted species and temperature profiles for an oxygen-enriched diffusion flame: 30% O_2 -70% N_2 vs. 20% CH_4 -80% N_2 , $\kappa = 60 \text{ s}^{-1}$. Numerical simulation using the GRI-3.0 mechanism.

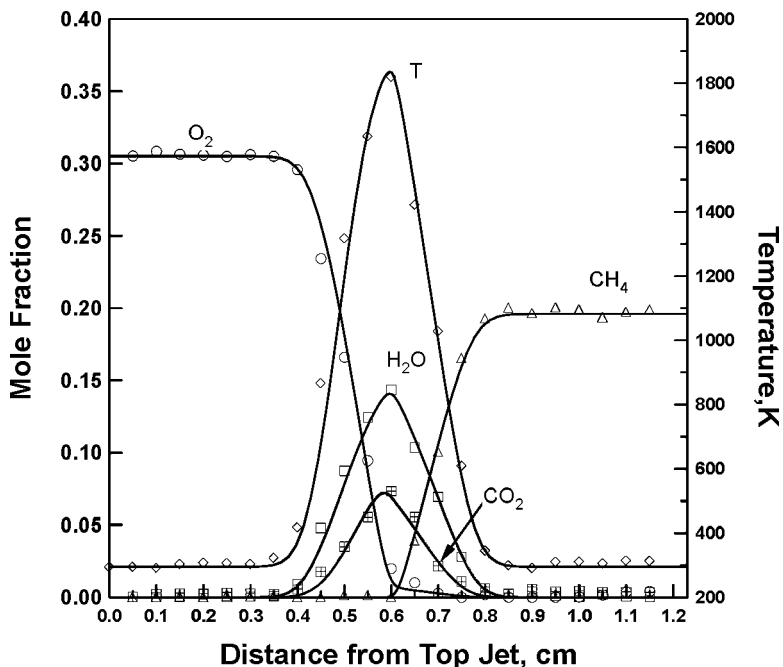


Figure 4. Experimental and numerically-predicted species and temperature profiles for an oxygen-enriched diffusion flame: 31% O_2 –69% N_2 vs. 20% CH_4 –80% N_2 , $\kappa = 130 \text{ s}^{-1}$. Numerical simulation using the GRI-3.0 mechanism.

Each flame has the similar reactant concentration (oxidizer jet is 30% O_2 –70% N_2 and fuel jet is 20% CH_4 –80% N_2), but at different stretch rate. Figure 3 shows the flame structure at stretch rate $\kappa = 60 \text{ s}^{-1}$. It can be seen that major species (O_2 , CH_4 , H_2O and CO_2) and temperature have a good agreement based on the comparison of experimental data and predictions that use the GRI-3.0 chemical kinetic mechanism. The estimated measurement error is 3% based on measurement in a Hencken calibration burner. The error bars are added for the representative data points in Figure 3. The measured peak temperature is 1883 K (± 57 K); the measured peak CO_2 is 7.4% ($\pm 0.22\%$); the measured peak H_2O is 13.1% ($\pm 0.39\%$). The flame thickness is 3.0 mm, based on the full width at half-maximum of the temperature profile.

With the stretch rate increasing to $\kappa = 130 \text{ s}^{-1}$, the flame structure is shown in Figure 4. Again, there is very good agreement for temperature and species concentration based on data-model comparison. The peak

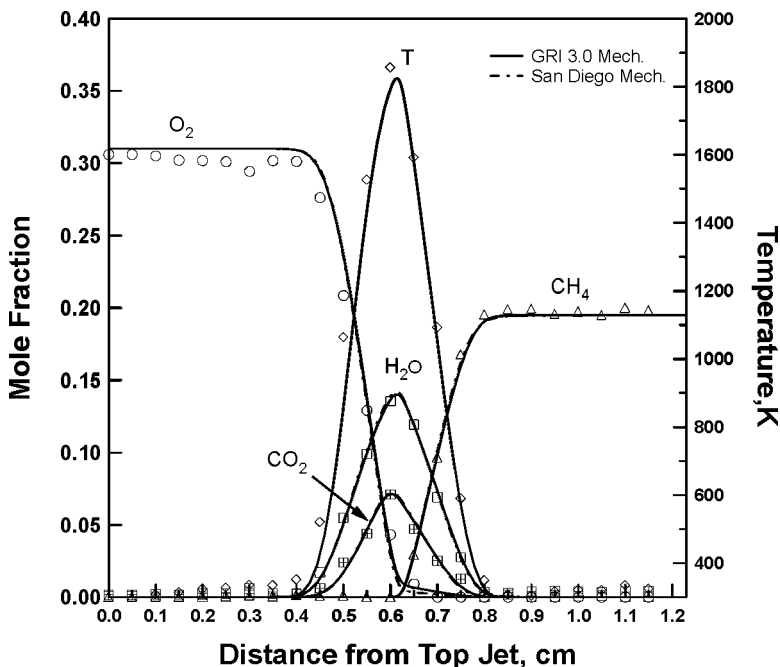


Figure 5. Experimental and numerically-predicted species and temperature profiles for an oxygen-enriched diffusion flame: 31% O_2 -69% N_2 vs. 20% CH_4 -80% N_2 , $\kappa = 168 \text{ s}^{-1}$. Numerical simulation using the GRI-3.0 and the San Diego mechanisms.

temperature is almost unchanged (1819 K) even though the stretch rate is doubled. The GRI-3.0 chemical kinetic mechanism works very well. Obviously the flame thickness (about 2 mm) decreases at this higher stretch rate. Continuing to increase stretch rate to $\kappa = 168 \text{ s}^{-1}$, the flame becomes thinner and the flame structure is shown in Figure 5. The model-data comparison shows an excellent match. The GRI-3.0 and the San Diego mechanisms are used for numerical simulation for this flame. Identical results are obtained for both chemical kinetic mechanisms which is not surprising as this is a non-premixed flame where the rate of combustion is controlled by the rate of diffusion of the fuel into the oxidizer. The specific reaction mechanism should not be very important except very near extinction.

In order to show the effect of the stretch rate and O_2 concentration on the flame structure, the temperature profiles for $\kappa = 60$ and 168 s^{-1} are shown in Figure 6. At $\kappa = 168 \text{ s}^{-1}$ and 30% O_2 , the temperature

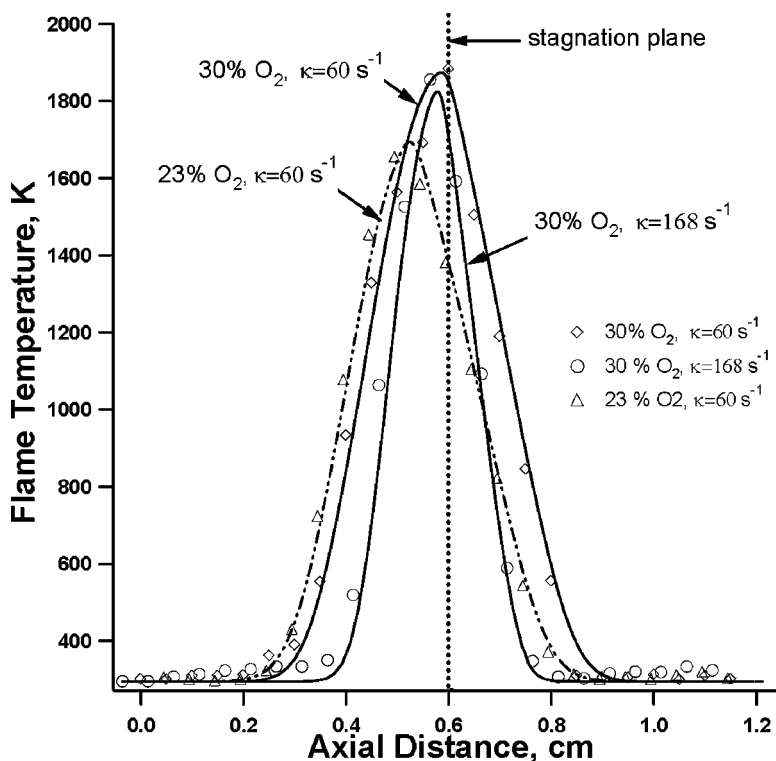


Figure 6. Stretch effect and oxygen concentration effect on temperature profiles (Fuel: 20% CH_4 -80% N_2). Numerical simulation using the GRI-3.0 mechanism.

slightly drops and the flame zone (thickness) becomes narrower than that at $\kappa = 60 \text{ s}^{-1}$ condition. Further, to identify the oxygen enhanced effect while maintaining the stretch rate at $\kappa = 60 \text{ s}^{-1}$, the oxygen concentration is lowered to 23%. It is found that when the oxygen concentration is close to 23%, the flame is near extinction for $\kappa = 60 \text{ s}^{-1}$. As seen in Figure 6, there is a 200 K temperature drop and the flame thickness increases when oxygen concentration changes from 30% to 23%. Further experiments indicate that no flame exists when using air (21% O_2) as the oxidizer at this stretch rate ($\kappa = 60 \text{ s}^{-1}$), which is consistent with the measurements by Ishizuka and Tsuji (1981). The enriched oxygen “strengthens” the combustion because of a reduced amount of inert nitrogen in the reactant. Also, there is a significant drop in the calculated NO concentration (from 105 ppm to 70 ppm) when the stretch rate

increases from 60 s^{-1} to 168 s^{-1} . This is because of reduced residence time and the slight temperature decrease.

Oxygen Concentration Effect on the Structure of Oxygen-Enhanced Flames

Oxygen is an important and common oxidizer. When an oxygen-enriched mixture is used as the oxidizer instead of air, less nitrogen dilution in reactants will cause the flame temperature to increase significantly. This is one of the most important features for the oxygen-enriched flame. For oxygen concentration from 31% to 100%, the detailed flame structures are shown in Figure 3 and Figures 7–9. Figure 7 shows the detailed flame structure for the opposed jet flow where one jet has a 41% O_2 –59% N_2 oxidizer stream and the other jet has a 20% CH_4 –80% N_2 fuel stream.

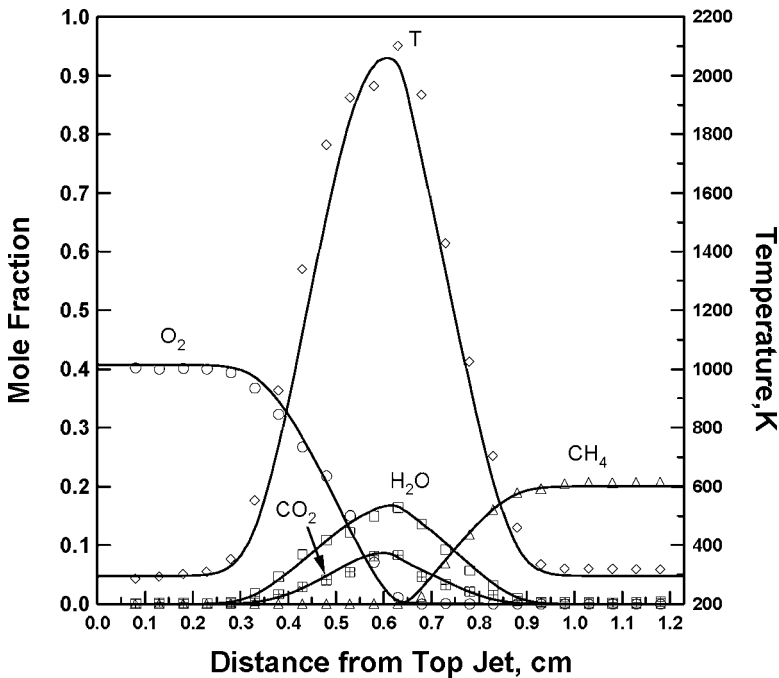


Figure 7. Experimental and numerically-predicted species and temperature profiles for an oxygen-enriched diffusion flame: 41% O_2 –59% N_2 vs. 20% CH_4 –80% N_2 , $\kappa = 60 \text{ s}^{-1}$. Numerical simulation using the GRI-3.0 mechanism.

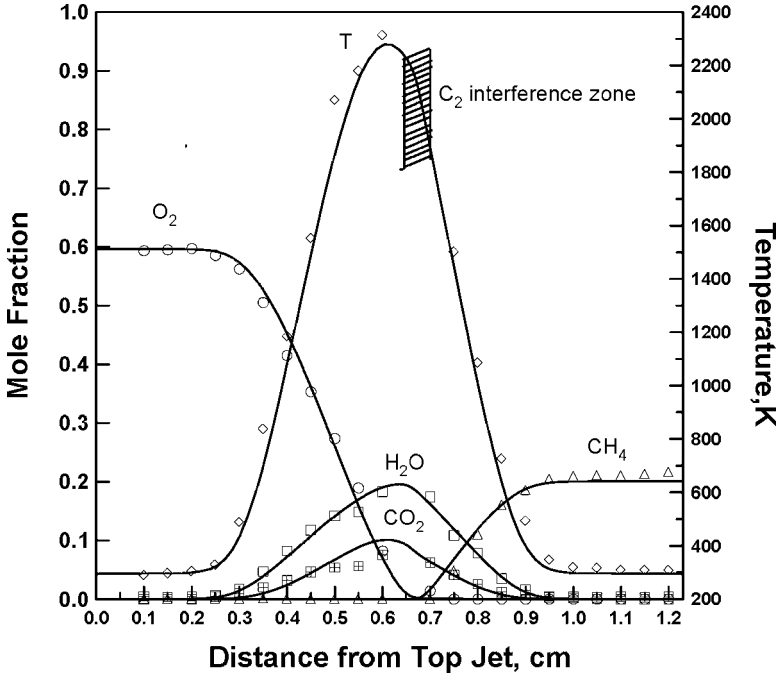


Figure 8. Experimental and numerically-predicted species and temperature profiles for an oxygen-enriched diffusion flame: 60% O_2 -40% N_2 vs. 20% CH_4 -80% N_2 , $\kappa = 60 \text{ s}^{-1}$. Numerical simulation using the GRI-3.0 mechanism.

The reason for using diluted fuel is that pure CH_4 produces significant interferences (i.e., laser-induced fluorescence of PAH) for the laser-based Raman measurement. From Figure 7, the calculated peak flame temperature is close to 2100 K. The measured species concentration profiles for O_2 , CH_4 , H_2O have a good agreement with the simulation using the GRI-3.0 chemical kinetic mechanism. In the flame zone, interference caused by C_2 emissions is much stronger than the 31% O_2 case. So the measured temperature slightly deviates from the simulated temperature. The measured CO_2 species concentrations have good agreement with the modeling results.

The flame structure with a 60% O_2 -40% N_2 oxidizer stream is shown in Figure 8. With the increasing amount of O_2 , the peak temperature rises to 2300 K. The agreement between data and numerical results are still good for O_2 , CH_4 , and H_2O , but the LIF interference (from C_2 ,

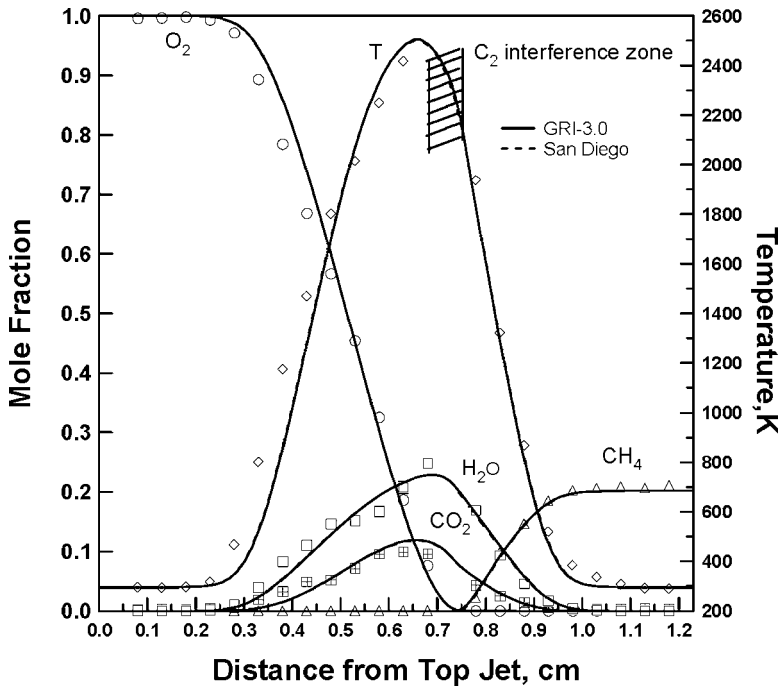


Figure 9. Experimental and numerically-predicted species and temperature profiles for an oxy/fuel diffusion flame: 100% O₂ vs. 20% CH₄-80% N₂, $\kappa = 60 \text{ s}^{-1}$. Numerical simulation using the GRI-3.0 and the San Diego mechanisms.

soot or PAH) on the fuel stream side (near flame zone) causes unreliable experimental data (in shadowed region). Interference from the C₂ Swan band has been seen previously in Raman spectra in hydrocarbon flames (Barlow et al., 2002) and in this work as well (see Figure 2c). Because this region is slightly off the region of peak flame temperature and it is only limited to a very small region, most of data are still reliable. The experimental CO₂ data slightly deviates from the simulated results near the center of the flame.

The calculated concentration level of NO increases to 500 ppm when the oxidizer varies from 30% O₂ (corresponding to 105 ppm NO) to 60% O₂. The oxygen-enhanced flame has this adverse potential to increase NO significantly when the oxygen concentration is less than 100% (Sung and Law, 1998). Figure 9 shows the flame structure for 100% O₂ vs. diluted CH₄. For this extreme case, the calculated flame temperature is 2503 K, a

value much greater than the adiabatic temperature of CH₄-air flames. The measured peak flame temperature (excluding the shadowed region) is 2416 K (± 63 K). The CO₂ and H₂O product concentrations increase significantly. Again, strong interference on the fuel stream side causes the experimental data to be unreliable in this limited region (see shadowed region and corresponding Raman spectra in Figure 2c). Outside of the thin interference zone, the measured species and temperature are in excellent agreement with modeling except that the CO₂ concentration is slightly over-predicted. The San Diego mechanism has also been used for simulation and gives nearly identical profiles for species and temperature to those obtained with the GRI-3.0 chemical kinetic mechanism. As stated before, since non-premixed flames are diffusion-controlled, the specific reaction mechanism should not have a strong effect on the flame structure except near flame extinction.

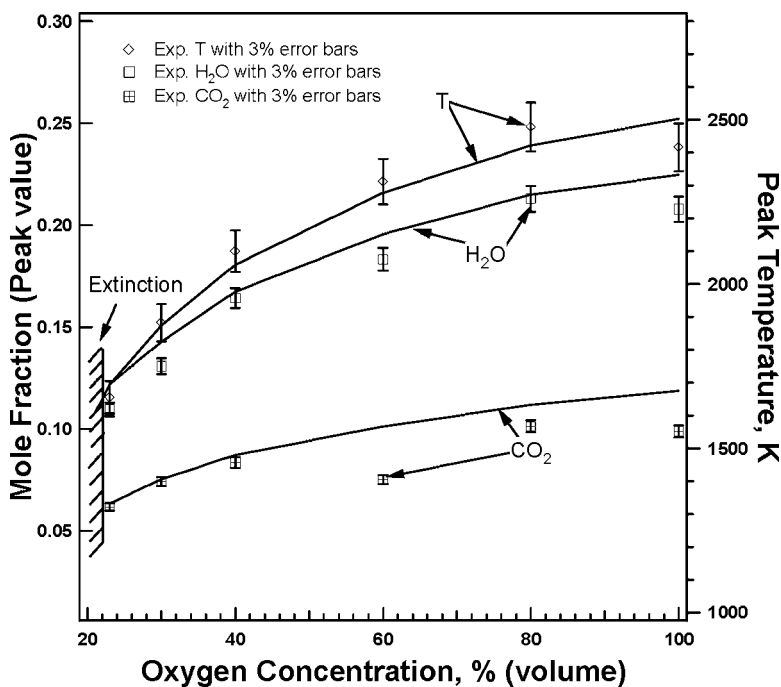


Figure 10. Oxygen concentration effect on temperature, H₂O and CO₂ profiles. Numerical simulation using the GRI-3.0 mechanism. The stretch rate is 60 s⁻¹ and the fuel stream is 20% CH₄-80% N₂.

Figure 10 summarizes the trend of CO_2 , H_2O and temperature with O_2 concentration in the oxidizer and shows these product concentrations increase with O_2 concentration. At the stretch rate $\kappa = 60 \text{ s}^{-1}$, the calculated peak flame temperature jumps from 1694 K to 2503 K when the O_2 concentration varies from 23% to 100%. The calculated CO_2 increases from 6.3% to 11.8% and calculated H_2O increases from 12% to 22% when the O_2 concentration changes from 23% to 100%. The experimental data for temperature and H_2O match with numerical results. However the measured CO_2 is slightly lower than the simulation results for 60%, 80% and 100% cases. This could be due to the difficulty of separating the O_2 and CO_2 Raman lines at high temperature (see Figures 2a and 2b where one CO_2 Raman line merges with the O_2 Raman line). Also in Figure 10, the lowest measured oxygen concentration (extinction limit) is given (23%) at a stretch rate of $\kappa = 60 \text{ s}^{-1}$ and a 20% CH_4 -80% N_2 fuel stream. The predicted value of 22% oxygen is nearly the same.

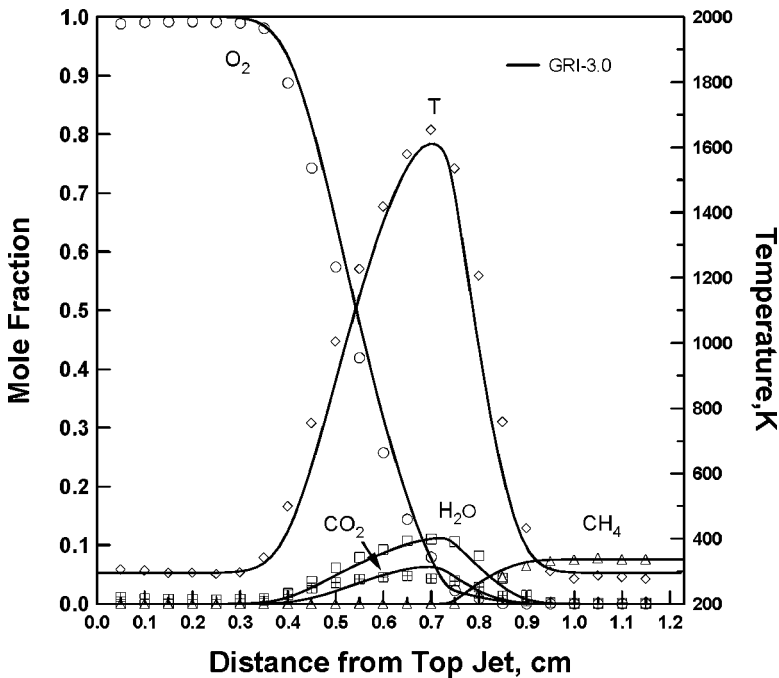


Figure 11. Experimental and numerically-predicted species and temperature profiles for an oxygen-enriched diffusion flame: 100% O_2 vs. 8% CH_4 -92% N_2 , $\kappa = 60 \text{ s}^{-1}$. Numerical simulation using the GRI-3.0 mechanism.

Flames Near the Extinction Limit

For diffusion flames, oxygen-enriched oxidizer can enhance combustion and may change the extinction limit. Figure 11 shows the flame structure for an extreme case: 100% O₂ stream vs. an 8% CH₄-92% N₂ stream with a stretch rate of $\kappa = 60 \text{ s}^{-1}$. Further decrease in the fuel concentration to 7% will cause the flame to go out. From Figure 11, it is found that peak flame temperature is only around 1600 K, even though the oxidizer is 100% O₂. Model-data comparisons show all reactants, products and temperature match very well. The predictions with the San Diego mechanism give the same results. Similarly, when the oxidizer is 100% O₂, the peak flame temperatures (both experimental data and numerical results predicted with two mechanisms) are given in Figure 12 with the CH₄ concentration varying from 7% to 20%. Just like varying oxidizer

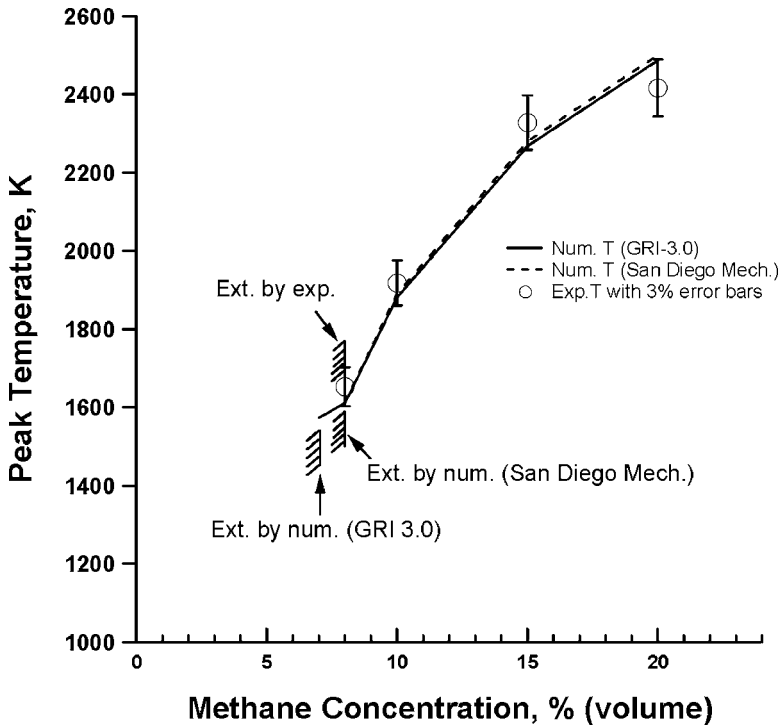


Figure 12. CH₄ concentration effect on temperature profiles when oxidizer is pure O₂. Stretch rate is 60 s^{-1} .

concentration, the fuel concentration changes the flame temperature significantly when 100% O₂ used as the oxidizer. The measured and predicted temperature results agree well with taking account of 3% uncertainty. If the fuel concentration is lower than 8%, the observed flame will go out. The numerical simulations predict a similar extinction limit: 7% CH₄ in N₂ with the GRI-3.0 mechanism and 8% CH₄ in N₂ with the San Diego mechanism (see Figure 12).

SUMMARY

Planar oxygen-enhanced counterflow methane flames are investigated by optical diagnostics and numerical simulation. The effects of stretch and oxygen concentration in the oxidizer on flame structure are studied in detail. The oxygen concentration of the reactants changes the flame temperature dramatically. At a constant stretch rate $\kappa = 60 \text{ s}^{-1}$, 1, there is about 800 K difference in flame temperature when oxidizer varies from 23% O₂ to 100% O₂. Simulations with the GRI-3.0 mechanism or the San Diego mechanism show that model-data comparisons for products such as H₂O and temperature agree very well. Interference from the C₂ Swan band on the fuel side disturbs the measurement for the high temperature oxygen-enhanced flame but only in very small range so the overall flame structure can still be investigated by the Raman measurement. The measured CO₂ values agree well with the predictions at lower oxygen enrichment (at 40% and below), but deviate at 60% oxygen enrichment and above. At high oxygen enrichment (60% and above), the temperature-induced shift of the Raman lines at high temperature leads to significant overlap of the O₂ and CO₂ Raman lines. The difficulty of separating these Raman lines at high temperature could contribute to the discrepancy between CO₂ measurements and predictions at high oxygen enrichment. At low-level enrichment (30% O₂), high stretch rate ($\kappa = 168 \text{ s}^{-1}$) or high-level oxygen-enrichment (100% O₂), low stretch rate ($\kappa = 60 \text{ s}^{-1}$), the GRI-3.0 and the San Diego mechanisms give almost identical predictions.

The effect of fuel concentration for pure oxygen flames is also studied. The measured extinction limit for the minimum amount of fuel in the diluted fuel mixture is close to the calculated value (using the GRI-3.0 mechanism or the San Diego mechanism) when pure oxygen is used as an oxidizer.

REFERENCES

- Barlow, R.S., Carter, C.D., and Pitz, R.W. (2002) Multiscalar diagnostics in turbulent flames. In Kohse-Höinghaus, K. and Jeffries, J.B. (Eds.) *Applied Combustion Diagnostics*, Taylor and Francis, New York, p. 384.
- Baukal, C.E. (1998) *Oxygen Enhanced Combustion*, CRC Press, Boca Raton, FL.
- Beltrame, A., Porshnev, P., Merchan-Merchan, W., Saveliev, A., Fridman, A., Kennedy, L.A., Petrova, O., Zhdanok, S., Amouri, F., and Charon, O. (2001) Soot and NO formation in methane-oxygen enriched diffusion flames. *Combust. Flame*, **124**, 295.
- Charon, O., Jouvaud, D., and Genies, B. (1993) Pulsated O₂/fuel flame as a new technique for low NO_x emission. *Combust. Sci. Tech.*, **93**, 211.
- Cheng, Z., Wehrmeyer, J.A., and Pitz, R.W. (2002) Opposed jet flames of lean premixed methane-air reactants vs. hot products, *38th AIAA/ASME/SAE/ASEE Joint Propulsion Conference*, AIAA 2002-4021, Indianapolis, IN.
- Cheng, Z., Wehrmeyer, J.A., and Pitz, R.W. (2005) Lean or Ultra-Lean Stretched Planar Methane/Air Flames. *Proc. Combust. Instit.*, **30**, 285.
- Ishizuka, S. and Tsuji, H. (1981) An Experimental Study of Effect of Inert Gases on Extinction of Laminar Diffusion Flames. *Proc. Combust. Instit.*, **18**, 695.
- Kee, R.J., Rupley, F.M., Miller, J.A., Coltrin, M.E., Grcar, J.F., Meeks, E., Moffat, H.K., Lutz, A.E., Dixon-Lewis, G., Smooke, M.D., Warnatz, J., Evans, G.H., Larson, R.S., Mitchell, R.E., Petzold, L.R., Reynolds, W.C., Caracotsios, M., Stewart, W.E., Glaborg, P., Wang, C., Adigun, O., Houf, W.G., Chou, C.P., and Miller, S.F. (2002) Chemkin Collection, Release 3.7, Reaction Design, Inc., San Diego, CA.
- Kim, J.S., Libby, P.A., and Williams, F.A. (1992) On the displacement effects of laminar flames. *Combust. Sci. Tech.*, **87**, 1.
- Leung, K.M., Lindstedt, R.P., and Jones, W.P. (1991) A simplified reaction mechanism for soot formation in nonpremixed flames. *Combust. Flame*, **87**, 289.
- Naik, S.V. and Laurendeau, N.M. (2002a) Quantitative laser-saturated fluorescence measurements of nitric oxide in counter-flow diffusion flames under sooting oxy-fuel conditions. *Combust. Flame*, **129**, 112.
- Naik, S.V. and Laurendeau, N.M. (2002b) Laser-saturated and linear laser-induced fluorescence measurements of nitric oxide in counterflow diffusion flames under non-sooting oxygen-enriched conditions. *Combust. Sci. Tech.*, **174**, 1.
- Naik, S.V., Laurendeau, N.M., Cooke, J.A., and Smooke, M.D. (2003) Effect of radiation on nitric oxide concentration under sooting oxy-fuel conditions. *Combust. Flame*, **134**, 425.
- Pourkashanian, M., Yapp, L., and San Diego, A. (1990) The use of oxygen enrichment in combustion technology. *Proc. Instit. Energy*, Adam Hilger, Bristol, England, p. 301.

- Qin, W., Ren, J.-Y., Egolfopoulos, F.N., Wu, S., Zhang, H., and Tsotsis, T.T. (2000) Oxygen Composition Modulation Effects on Flame Propagation and NO_x Formation in Methane/Air Premixed Flames. *Proc. Combust. Instit.*, **28**, 1825.
- Seshadri, K., Puri, I., and Peters, N. (1985) Experimental and theoretical investigation of partially premixed diffusion flames at extinction. *Combust. Flame*, **61**, 237.
- Smith, G.P., Golden, D.M., Frenklach, M., Moriarty, N.W., Eiteneer, B., Goldenberg, M., Bowman, C.T., Hanson, R.K., Song, S., Gardiner, Jr., W.C., Lissianski, V.V., and Qin, Z. (1999) (http://www.me.berkeley.edu/gri_mech/)
- Sung, C.J. and Law, C.K. (1998) Dominant Chemistry and Physical Factors Affecting NO Formation and Control in Oxy-Fuel Burning. *Proc. Combust. Instit.*, **27**, 1411.
- Sung, C.J., Liu, J.B., and Law, C.K. (1995) Structural response of counterflow diffusion flames to strain rate variations. *Combust. Flame*, **102**, 481.
- Vandsburger, U., Kennedy, I., and Glassman, I. (1984) Sooting counterflow diffusion flames with varying oxygen index. *Combust. Sci. Tech.*, **39**, 263.
- Williams, F.A. (2003) San Diego Mechanism (<http://maeweb.ucsd.edu/~combustion/cermech>) (2003/08/30).